Development and characterization of silicone embedded distributed piezoelectric sensors for contact detection

IOP Publishing Smart Materials and Structures
Smart Mater. Struct. 24 (2015) 075030 (15pp) doi:10.1088/0964-1726/24/7/075030

Development and characterization of silicone embedded distributed piezoelectric sensors for contact detection

Merve Acer[1], Marco Salerno[2], Kossi Agbeviade[3] and Jamie Paik[2]

[1] Department of Mechanical Engineering, Istanbul Technical University, Beyoğlu 34437, Istanbul, Turkey
[2] Reconfigurable Robotics Laboratory, Swiss Institute of Technology, Lausanne EPFL, CH-1015 Lausanne, Switzerland
[3] Mechanical System Design Laboratory, Swiss Institute of Technology, Lausanne EPFL, CH-1015 Lausanne, Switzerland

E-mail: acerm@itu.edu.tr and jamie.paik@epfl.ch

Received 8 February 2015, revised 14 April 2015
Accepted for publication 8 May 2015
Published 17 June 2015

Abstract

Tactile sensing transfers complex interactive information in a most intuitive sense. Such a populated set of data from the environment and human interactions necessitates various degrees of information from both modular and distributed areas. A sensor design that could provide such types of feedback becomes challenging when the target component has a nonuniform, agile, high resolution, and soft surface. This paper presents an innovative methodology for the manufacture of novel soft sensors that have a high resolution sensing array due to the sensitivity of ceramic piezoelectric (PZT) elements, while uncommonly matched with the high stretchability of the soft substrate and electrode design. Further, they have a low profile and their transfer function is easy to tune by changing the material and thickness of the soft substrate in which the PZTs are embedded. In this manuscript, we present experimental results of the soft sensor prototypes: PZTs arranged in a four by two array form, measuring 1.5–2.3 mm in thickness, with the sensitivity in the range of 0.07–0.12 of the normalized signal change per unit force. We have conducted extensive tests under dynamic loading conditions that include impact, step and cyclic. The presented prototype's mechanical and functional capacities are promising for applications in biomedical systems where soft, wearable and high precision sensors are needed.

Keywords: tactile sensor array, force sensors, soft sensors, piezoelectric

(Some figures may appear in colour only in the online journal)

1. Introduction

Tactile sensing requires small sensor feature sizes to maintain sensitivity, particularly for diverse applications including robotics, where sensitivity and precision are needed to perform tasks that entail physical interaction with the environment. By elaborating force and pressure information, tactile sensors have the capability to measure parameters such as friction, stiffness and force localization. Thus, the contact interaction between the sensor and the environment can be identified [1]. These sensors and their applications are highly desired in human-robot interaction [2, 3], biomedical robotics [4, 5] and biomimetic robotics [6] in order to provide effective sensory feedback.

Various typologies of tactile and force sensors that provide contact detection, localization of forces, force measurements, strain measurements and object recognition can be found in the literature [1]. However, it is rare to find methodologies for the design of miniaturized tactile sensors allowing customization, tunable sensitivity and, more importantly, softness and flexibility. Thin, stretchable, soft and high accuracy contact sensors are often sought after for applications in wearable robotics, where flexibility and adaptability are the target features of safe robotic systems, surgical tools and robotics [7]. A typical example of such sensors is represented by the human-robot interaction systems where artificial e-skins are required [3]. These sensors should

have the capability to provide a tactile sensation composed of sensitive distributed tactile pixels arrays. An effective solution could be covering these robotic parts with thin, highly sensitive, distributed, soft sensors. The main challenges for designing such sensors would be the capability to express high strain and flexibility in order to cover the complex shapes, and tunable resolution in order to increase the effectiveness, accuracy and safety.

The development of novel tactile sensors that are soft, sensitive, and distributable over a large area has attracted great research interest but remains a challenge. Flexible or soft tactile/force sensors mentioned in the literature have been developed using mostly optical [8–10], resistive [11–16], capacitive [17, 18], and piezoelectric [19–22] principles. Optical based sensors use a light source in an elastic medium and measure the change in the transmission or pattern of light when a force is applied [8–10]: they are mostly designed to be used in surgical instruments. Resistive sensors [11–16] and capacitive sensors [17, 18] measure the change of resistance and capacitance of the sensing material respectively and convert it to the applied force/pressure: they are mostly developed for wearable applications due to their material flexibility. Piezoelectric sensors use the dynamic voltage change of the piezoelectric material when it is deformed [19–22]: they are used in applications that require high frequency and sensitivity such as in biomedical vibrotactile systems.

Many optical sensors are composed of flexible yet brittle glass fibers that produce varying light reflection readings depending on the unwanted bending, with a consequent high risk of mechanical failure. An interesting solution to this issue, thus providing more flexibility to these systems, is represented by flexible optical sensors, fabricated using plastic optical fibers [7, 8]. These sensors are manufactured by embedding a 2D mesh of fibers in a silicone elastomer. Another flexible optical sensor has been developed in [9] using a thin photodiode and thin laser source without optical fibers. The sensor output is driven by the shear stresses on a deformable PDMS layer between the source and the diode. Optical sensors have the advantage of not being subject to crosstalk; however, signal disturbances may occur due to unwanted bending or misalignments.

Resistive sensors are the most common tactile sensors; they provide a change in electrical resistance related to an applied pressure/force. One of the most popular ways of introducing flexibility in sensors is by using conductive elastomers, conductive polymers and conductive liquids. Kim *et al* employed conductive polymers to design a flexible tactile sensor able to cover curved surfaces and to embed up to 32×32 sensitive elements with a size of 5.5×6.5 cm [10]. Carbon nanotubes (CNT) are another type of material employed in the design of resistive based tactile sensors. A 2×2 shear-sensing array developed in [11] uses CNTs and adapts MEMS polymer fabrication technology. The fabrication process comprises several steps including film deposition, lithography, etching and packaging. Piezoresistive composite films inserted in PDMS layers are used in [12, 13]. These materials are flexible, robust, economical and have a higher gauge factor compared to metal alloy strain gauges. However, their mechanical behavior is viscoelastic so they display nonlinearity and hysteresis. The other option for designing flexible tactile sensors is to use conductive liquid. Microchannels embedded in an elastomer are filled with conductive liquid expressing a resistive [14, 15] or a capacitive [16, 17] change when the cross sectional areas of the microchannels change. Capacitive sensors have a good linear response, high resolution and good dynamic properties compared to resistive sensors but the produced signals usually have a reduced resolution for array configurations and require complex signal conditioning. Conductive-liquid-based sensors provide softness and stretchability but they cannot be used in large areas and the fabrication process is quite complex for a highly populated sensing surface.

Piezoelectric domain sensors are, in principle, transducers that convert energy between mechanical and electrical energy in both directions. The sensitivity of piezoelectric elements is very high (15–65 nm V^{-1}) requiring much less signal conditioning compared to conventional strain gauges, especially in applications where there are low strains and high noise levels [18].

There are two main types of piezoelectric elements that are used as sensors: piezoelectric polymers and piezoelectric ceramics (PZT). In order to take advantage of its high flexibility, polyvinylidene fluoride (PVDF) is one of the most commonly used sensitive piezoelectric polymers [19–22]. Typical polymeric piezoelectric tactile sensors consist of a single PVDF layer with multiple electrodes. A micromachined silicon layer [19] and inkjet-printed silver pattern in arrays provide electric paths for localizing the applied forces [22]. To minimize the crosstalk affect in single layered sensors, Kim *et al* designed a tactile sensor showing distributed dome shapes in the PVDF layer [21], thus improving force localization. While these sensors provide sensitive force distribution measurements, they remain relatively stiff for covering complex surfaces.

In this paper, we present a novel soft sensor prototype consisting of PZT elements (figure 1) that measures the contact forces to provide tactile feedback. The main contributions of this work can be listed as follows.

- The sensor is composed, first, of discrete PZT elements that provide high accuracy and sensitivity that offer more robust signal reading compared to polymers and, second, of a soft silicone substrate that provides compliance in the soft sensor application.

  The embedding of sensing elements into a silicone layer causes the following main effects.
- Distributing separate sensing elements in a soft media enables the sensor to adapt to different surfaces. We present a sensor prototype with a 4×2 array of PZT elements embedded in silicone and localization of contact forces has been demonstrated successfully.
- The contact force applied is transmitted through the silicone substrate to pick up not only the normal, but also the shear, forces. Therefore, even a sensitivity in shear loading sliding input can be detected and deciphered by analyzing the activation sequence of different sensing

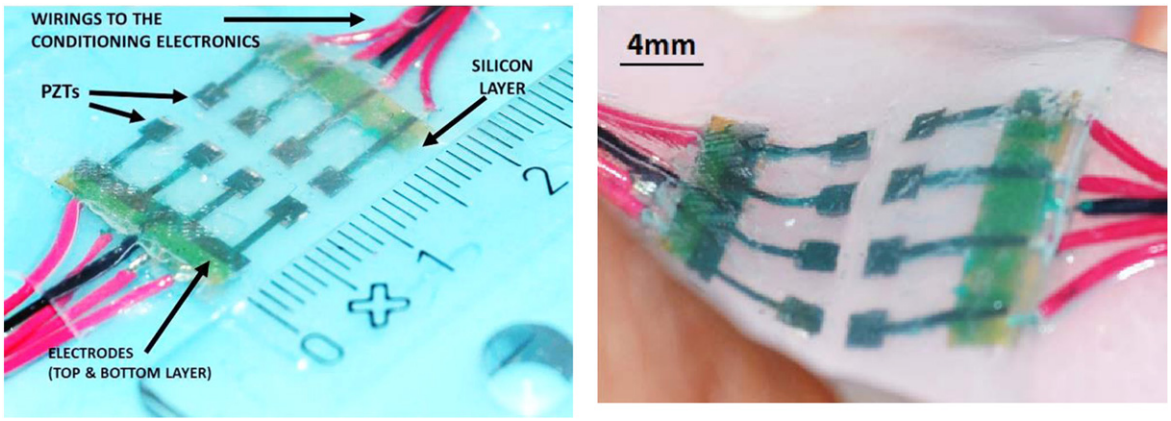

Figure 1. The soft tactile sensor prototype with distributed $2 \times 2\,\text{mm}^2$ PZT elements that can cover complex curved surfaces.

elements. This has been proved by performing a slide test with a specifically designed surface. The results showed the possibility of evaluating shear forces on the sensitive surface.

- Sensor transfer function tuning according to material embedment modifications (its thickness, stiffness and damping): the sensor has been modeled by combining the physical model of the PZT element and the elastic medium and the transfer function has been extracted theoretically. It has been observed that the elastic medium properties affect the transfer function. The developed sensor prototypes have two different substrate thicknesses, 1.5 mm and 2.3 mm, to demonstrate the tuning of the transfer function.

The paper is organized as follows: section 2 presents the theoretical and experimental methodologies for designing and characterizing the distribution and sensitivity of the sensor elements. Section 3 shows the characterization results of the prototype. In section 4 the results are discussed and section 5 concludes with a description of future work and applications of the presented soft sensor.

2. Theoretical modeling

PZT ceramic materials are not an obvious choice for bendable and soft tactile sensors because they are extremely brittle ($E = 8 \times 10^9\,\text{N m}^{-2}$), although they are very responsive to applied forces with a high sensitivity. In this paper the authors present a solution by embedding PZT elements in an elastic substrate that provides enough flexibility and softness and can even be used as a wearable sensor for contact detection and force measurement. In this section the effect of silicone embedment of PZT sensors has been investigated with our theoretical methods and the signal conditioning for the amplification and filtering of PZT voltage outputs is explained.

The silicone embedment has been formulated combining the general PZT sensor equations using an equivalent electric circuit with the mechanical model of the PZT sensor embedded in elastic material. The elastic material has been described with the Kelvin–Voigt model, the effect of the elastic material thickness change has been analyzed and then compared with the experimental results. We will also present the model for the potential maximum density of PZT elements in the elastic media.

2.1. PZT sensor modeling

When the PZT ceramic is under loading, the crystal atoms are displaced. This displacement, x, is proportional to the applied force, F, with a constant, k, which is the stiffness of the material.

$$x = \frac{1}{k}F. \tag{1}$$

PZT ceramic is a brittle material and its elastic modulus is high ($8 \times 10^9\,\text{N m}^{-2}$) which means that k is very large for the PZT ceramics. The deformation produces a net charge, q, proportional to x

$$q = Kx. \tag{2}$$

From equations (1) and (2) the following relation is found, which is called the 'direct piezoelectric effect' [23]:

$$q = \frac{K}{k}F \tag{3}$$

where K/k is the piezoelectric constant, e_{33}. The PZT element can be represented as a charge generator q in parallel to a capacitance C_s which depends on the ε_0, the dielectric constant of free space ε_r, the relative dielectric constant of PZT, A, the area of the surface, and, t, the thickness [24].

$$C_s = \varepsilon_0 \varepsilon_r \frac{A}{t}. \tag{4}$$

The equivalent electric circuit of the PZT element is shown in figure 2, according to Kirchhoff's current law:

$$i_s = \frac{\mathrm{d}q}{\mathrm{d}t} = K\frac{\mathrm{d}x}{\mathrm{d}t} \tag{5}$$

$$i_s = i_c - i_R \quad i_c = i_s - i_R \tag{6}$$

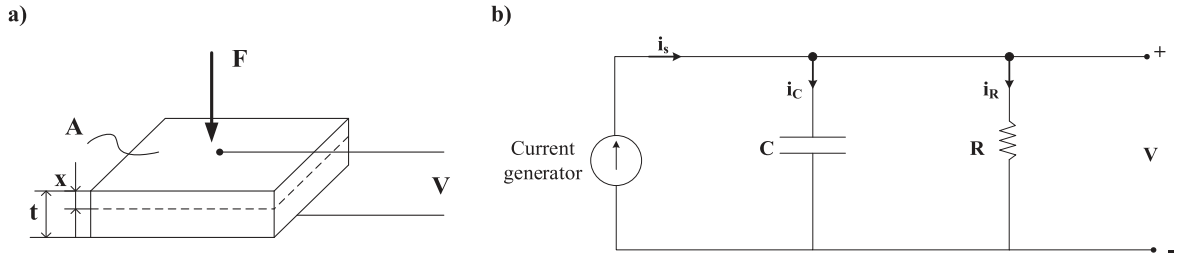

Figure 2. (a) Single PZT element under loading. (b) Equivalent electric circuit of PZT element.

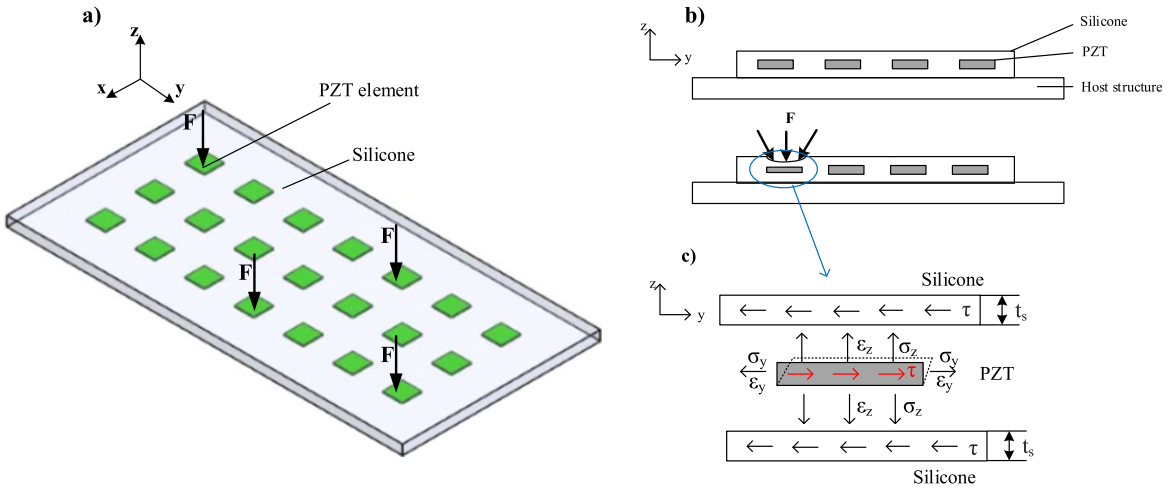

Figure 3. (a) Distributed PZT elements embedded in silicone subjected to distributed forces. (b) Front view of the sensor when one PZT element is subjected to a force. (c) Activated PZT element free body diagram.

If connected to an amplifier, we have:

$$C\left(\frac{\mathrm{d}V}{\mathrm{d}t}\right) = K\frac{\mathrm{d}x}{\mathrm{d}t} - \frac{V}{R} \tag{7}$$

where $C = C_s + C_c + C_a$, $R \approx R_a$, C_c is the parasitic capacitance input of the connection cables, C_a is the amplifier input capacitance and R_a is the amplifier resistance which is much greater than the resistance of the cable.

A general transfer function that relates the deformation of the PZT element to the generated voltage is found as:

$$G_1(s) = \frac{V(s)}{X(s)} = \frac{K_s \tau s}{\tau s + 1} \tag{8}$$

where $K_s = K/C$ is the sensitivity and $\tau = RC$ is the time constant.

2.2. PZT sensor physical modeling embedded in silicone

The developed sensor is composed of distributed PZT elements embedded in silicone (figure 3(a)) in order to measure and localize the contact forces. When the elastic medium that covers the PZT elements is subjected to a force or pressure (figure 3(b)), the corresponding PZT elements are subjected to shear τ and normal stresses σ_z as shown in figure 3(c).

The constitutive 2D stress-strain relations for the electromechanical behavior of a single PZT element which is poled in the z direction can be described as follows:

$$\sigma_y = c_{11}\varepsilon_y + c_{31}\varepsilon_z - e_{31}E_z \tag{9}$$

$$\sigma_z = c_{31}\varepsilon_y + c_{33}\varepsilon_z - e_{33}E_z \tag{10}$$

$$D_z = e_{13}\varepsilon_y + e_{33}\varepsilon_z - \lambda_{33}E_z \tag{11}$$

where the stress and strain components which are assumed to be uniformly distributed across the thickness are σ_y, σ_z, ε_y and ε_z. D_z is the electric displacement field, c_{11}, c_{31}, and c_{33} are the elastic compliances, e_{31} and e_{33} are the piezoelectric constants, λ_{33} is the dielectric constant and E_z is the electric field. The static and dynamic models for the PZT elements in the elastic media using these stress-strain equations are adopted from the equations for the two dimensional plane where the elastic material is considered as an homogeneous and isotropic elastic insulator [25–28]. According to the theoretical results of their work, the voltage along the PZT element depends on the material and geometric properties of elastic media which significantly affect the shear stress that changes the transverse stresses and axial strains.

The Kelvin–Voigt model has been used to model the silicone in which the material is represented by a damper (b_s) and a spring (k_s) in parallel in order to write a transfer function that relates the input displacement (x_1) of the silicone caused by the contact force (F) to the deformation of the PZT element (x_2).

From the equilibrium of forces at point 1 (figure 4(a)):

$$F = -b_s\dot{x}_1 - k_s x_1. \tag{12}$$

The equation of motion of a PZT can be defined by using a second order differential equation with a mass, m_p, spring, k_p, and a damper, b_p [22]. So the equilibrium of forces for the

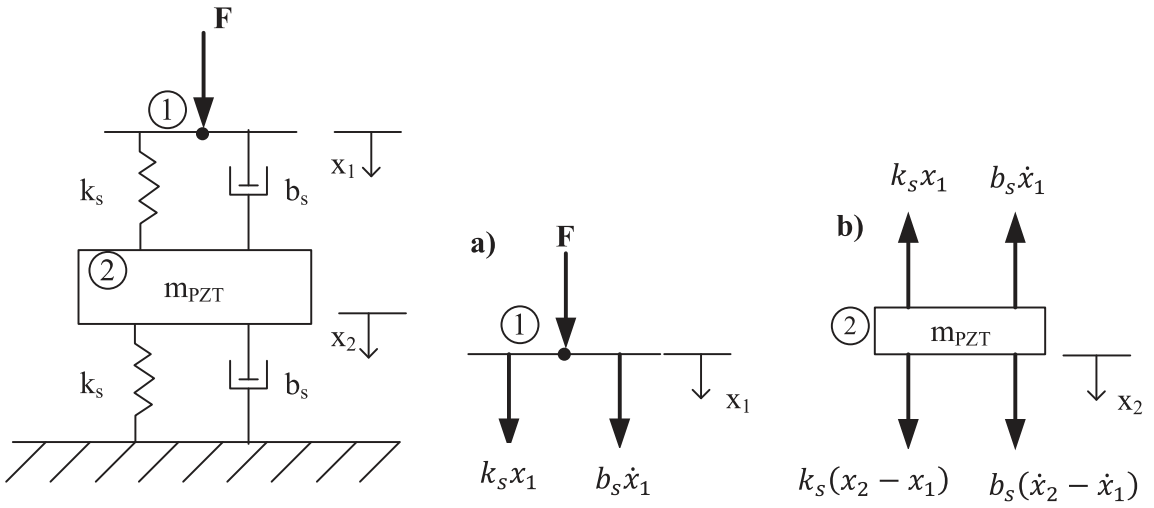

Figure 4. Model of the single PZT sensor embedded in silicone. The free body diagram of point 1 which is the point of force acting on the silicone (a) and free body diagram of the PZT element inside the silicone (b).

PZT embedded in silicone (see figure 4(b)) can be written as:

$$m_P\ddot{x}_2 + b_p\dot{x}_2 + k_p x_2 + b_s(\dot{x}_2 - \dot{x}_1) + k_s(x_2 - x_1) - b_s\dot{x}_1 - k_s x_1 = 0 \quad (13)$$

$$m_P\ddot{x}_2 + \underbrace{(b_p - b_s)}_{b_{eq}}\dot{x}_2 + \underbrace{(k_p - k_s)}_{k_{eq}}x_2 = 2b_s\dot{x}_1 + 2k_s x_1 \quad (14)$$

The left hand side of equation (14) gives the PZT dynamics inside the silicone, where b_p–b_s is the equivalent damping factor and k_p–k_s is the equivalent stiffness, and the right hand side gives the applied force on the PZT element when there is a contact on the silicon which deforms the surface as x_1. The transfer function that relates input x_1 to PZT deformation x_2 can be reorganized and written as follows:

$$G_2(s) = \frac{X_1(s)}{X_2(s)} = \frac{(2/k_{eq})(b_s s + k_s)}{(s^2 + 2\zeta\omega_n s + \omega_n^2)} \quad (15)$$

where $k_{eq} \approx k_p$ because the stiffness of PZT is very large, $\omega_n = \sqrt{k_p/m_p}$ and $\zeta = b_{eq}/(2\sqrt{k_p m_p})$.

Finally, using equations (8) and (15), the transfer function in which displacement x_1 of the silicone is the input and the voltage generated by the PZT embedded in silicone material is the output, is found as:

$$G(s) = \frac{V(s)}{X_1(s)} \cdot \frac{X_1(s)}{X_2(s)} = G_1(s) \cdot G_2(s) = \frac{K_s\tau s}{\tau s + 1} \cdot \frac{(2/k_p)(b_s s + k_s)}{(s^2 + 2\zeta\omega_n s + \omega_n^2)} . \quad (16)$$

The parameters b_s and k_s depend on the elastic material properties viscosity, μ, and the elastic modulus, E, respectively, so the properties of the elastic medium changes the transfer function of the sensor. The material properties also depend on the area, A_e, and thickness, t_e, of the material.

$$b_s = \frac{\mu}{t_e} \cdot A_e, \qquad k_s = \frac{E_e}{t_e} \cdot A_e . \quad (17)$$

Table 1. The parameters of PZT and silicone.

Parameters of PZT	Parameters of silicone
$e_{33} = 110 \times 10^9$ C N^{-1}	$E_e = 8 \cdot 10^6$ N m^{-2}
$E_p = 8 \cdot 0^9$ N m^{-2}	$M = 10$
$A = 4 \cdot 10^{-6}$ m^2	$A_e = 4 \cdot 10^{-6}$ m^2
$R = 160$ kΩ	$t_e = 0.05$–0.5 mm
$C = 610$ pF	
$Z = 1$	
$\omega_n = 63$	

In this work we have characterized the sensitivity of the PZT sensor embedded in silicone with different thicknesses. With the transfer function, equation (16), and theoretical parameters of the sensor (table 1) the relation between the output voltage and a stepwise change of the input force depends on the thickness of silicone ($t_e = 0.05$–0.5 mm as shown in figure 5) due to the b_s and k_s parameter changes.

2.3. PZT distribution in elastic media

One of the most significant design contributions of the presented sensor prototype is the distribution and localization of forces on detectable areas. This sensor reading is not limited to the direct localized application of the force on the PZT elements surface, but thanks to the soft medium, it provides continuous tactile feedback with discrete sensing elements even where the PZT element is not present. Distribution of these elements inside the elastic material is a crucial element in order to distinguish the signals from those of the neighboring PZT elements. It is considered that a point force is applied on the center of the surface of a single PZT element as shown in figure 6 and the elastic material is taken as a plate.

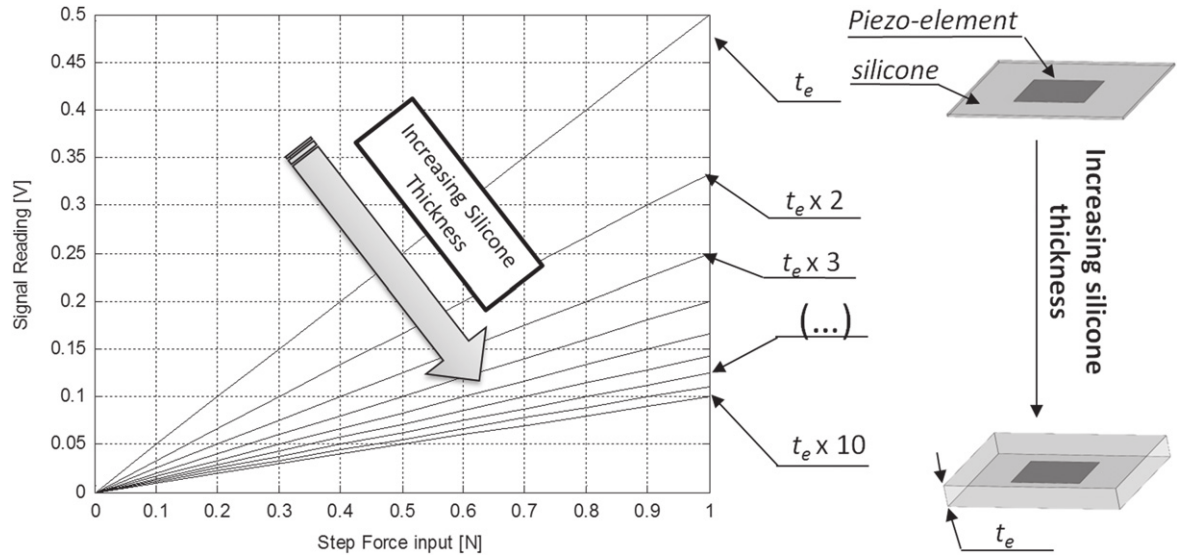

Figure 5. Dependence of the transfer function of the PZT on the thickness of the elastic material.

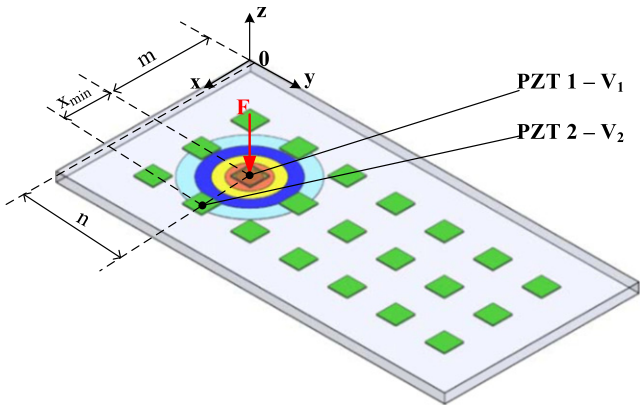

Figure 6. Top view of distributed PZT sensor embedded in elastic material with impact forces F acting on the center point of PZT surfaces.

When the force is applied, the deformation (u_z) on the plate travels like a spherical wave along the surface. The displacement between the PZTs in the x and y axes will be the same considering the deformation distribution as spherical; in this section we will provide a formulation for calculating $x_{\min}$.

The difference between the output voltages of the neighboring elements and the activated element should not be lower than the resolution of the electronic system in order to distinguish the values and localize the force. Therefore, when a force is applied on PZT 1 as shown in figure 6, the difference of the voltage output, V_1, and the neighboring voltage output PZT 2, V_2, should be:

$$V_1 - V_2 = \Delta V \tag{18}$$

where ΔV is the resolution of the electronic system. According to the minimum voltage outputs from PZT 2 the minimum deformation needed on the PZT sensor can be calculated by using the model equation (7) as follows:

$$C\left(\frac{\mathrm{d}\left(V_1 + \Delta V\right)}{\mathrm{d}t}\right) = K\frac{\mathrm{d}u_z}{\mathrm{d}t} - \frac{V_1 + \Delta V}{R} \tag{19}$$

$$\frac{\mathrm{d}u_z}{\mathrm{d}t} = \frac{1}{K}\left(C\left(\frac{\mathrm{d}\left(V_1 + \Delta V\right)}{\mathrm{d}t}\right) + \frac{V_1 + \Delta V}{R}\right) \tag{20}$$

where u_z is the deformation.

The distribution of the deformation due to the applied force can be calculated by using the general wave equation for the thin flexible plates that are subjected to forces:

$$m\frac{\partial^2 u_z(x, y, t)}{\partial t^2} + \beta\frac{\partial u_z(x, y, t)}{\partial t} + D\Delta^2 u_z(x, y, t) = q(m, n, t)\,, \tag{21}$$

where m is the surface mass density, β is the damping factor, Δ is the Laplacian operator, $q(x,y,t)$ is the applied force on the point (m,n) and D is the bending stiffness which depends on the elastic modulus E, the Poisson ratio ν and the plate thickness t_e:

$$D = \frac{Et_e^3}{12\left(1 - \nu^2\right)}. \tag{22}$$

The solution of $u(x,y,t)$ for the impact force, $q(m, n, t) = \delta(m)\delta(n)\delta(t)$ is presented in [28]. The deformation along the flexible plate $u_z(x, y, t)$ and the derivative of the deformation $\dot{u}_z(x, y, t)$ is found in [29] as:

$$u_z(x, y, t) = \frac{1}{m\sqrt{2\pi}}\int_{-\infty}^{\infty}\int_{-\infty}^{\infty}\frac{1}{\gamma k^2\sqrt{1 - \zeta^2}}A \cdot B\mathrm{d}k_x\mathrm{d}k_y$$
$$A = \mathrm{e}^{-\zeta\gamma k^2 t}\sin\left(\gamma k^2 t\sqrt{1 - \zeta^2}\right),\ B = \mathrm{e}^{\mathrm{i}\left(k_x x + k_y y\right)} \tag{23}$$

where $\gamma = \sqrt{\frac{D}{m}}$, $\zeta = \frac{\beta}{2m\gamma k^2}$, $k = k_x^2 + k_y^2$, and k_x and k_y are the spatial wave numbers along the x and y axes, respectively, which is explained in [28].

Finally, for our case where we are interested in a matrix of pixels, $x_{\min}$ can be calculated as:

$$\frac{\partial u_z(x_{\min}, n, t)}{\partial t} = \frac{1}{K}\left(C\left(\frac{\mathrm{d}(V_\mathrm{l} + \Delta V)}{\mathrm{d}t}\right) + \frac{V_\mathrm{l} + \Delta V}{R}\right). \quad (24)$$

Equation (24) presents the formulation of the optimization problem for calculating the minimum distance between PZT elements. For our case the minimum voltage difference between the PZT pixels should be 1.2 mV because of our DAQ limitations. Solving equation (24), the minimum deformation $u_{z\min}$ that can be sensed by the pixels is 0.027 nm. Here we will not go into the detail of solving equation (24) which is presented in [29] but by solving equation (23) the minimum distance between the pixels can be found. Besides the manufacturing processes, for the wiring electrodes at the top and bottom layers of each PZT element, the insulation of wiring should be taken into account while designing these sensors.

2.4. Signal conditioning

The general electrical model of the PZT sensor has already been presented in section 2.1, however, for the force measurement application, it is more convenient to use a charge mode amplifier, or to convert the produced charges into voltage with a high impedance voltage amplifier. The proposed design using a TLV 2772 operational amplifier, (see figure 7(a)), offers the possibility to work in individual modes or to combine both modes. In such a case, the first stage works as voltage mode converter and the second one as low-pass filter.

Figure 7(b) details the connection between the sensor and the amplifier. The following assumptions have been made for the circuit design.

- The internal resistor R_p of the sensor source is very high.
- The internal parallel resistor R_c of the cable is very high.
- The op-amp has a CMOS input stage so its input resistance, R_i, is very high.

It can be concluded that the currents flowing through the resistors are negligible. Therefore, the voltage at the input of the operational amplifier can be calculated as in equation (25) using the charge of the PZT, Q_p, and capacitances of the PZT, C_p, cable, C_c and op-amp input, C_i.

$$V_\mathrm{e} = \frac{Q_\mathrm{p}}{C_\mathrm{p} + C_\mathrm{c} + C_\mathrm{i}}. \quad (25)$$

The PZT capacitance measurement has been performed with three samples and the mean value for C_p has been found to be 875 pF, which is much higher than the cable and op-amp input capacitance values. Therefore, the output voltage can be found as $V_\mathrm{e} = Q_\mathrm{p}/C_\mathrm{p}$.

The full schematics of the charge amplifier and low-pass filter in figure 7(c) is reduced to figure 7(d) according to the following assumptions:

- as before, R_p, R_c, R_i are very high;
- R_i must be sufficiently small to avoid significant voltage drop at its ends when charges are flowing;
- feedback resistance, R_f, should be large enough to force major charge flow through the feedback capacitance C_f;
- the gain A of the op-amp is very high;
- The op-amp input current is null due to its high input impedance.

By applying Kirchoff's law to figure 10(d) for a TLV 2772A the gain A is at least 80 dB (10^4). Therefore, the output voltage is:

$$V_\mathrm{s} = -\frac{Q_\mathrm{p}}{C_\mathrm{f}}. \quad (26)$$

Here appears the main advantage of the charge amplifier. All external parasitic effects are suppressed. Only the charge Q_p produced by the sensor remains and is transferred to C_f.

$-1/C_\mathrm{f}$ is the gain of the charge amplifier. Considering figure 10(a), the output signal of the first stage is a voltage, proportional to the charge sensed by the PZT. This voltage can be applied to the second stage, which will then act as a low-pass filter with a gain of $G_\mathrm{lp} = -\frac{Z_\mathrm{f}}{R'_\mathrm{i}}$. where R'_i is the external input resistor and Z_f is the feedback impedance as:

$$G_\mathrm{lp} = -\frac{R_\mathrm{f}}{R'_\mathrm{i}}\frac{1}{1 + j\omega\tau_\mathrm{f}} \quad (27)$$

which is a first order low-pass filter. The stic gain is given by $\frac{R_\mathrm{f}}{R'_\mathrm{i}}$ and the cut-off frequency can be calculated from $\omega = \frac{1}{\tau_\mathrm{f}}$. For our application where $R_\mathrm{f} = 390\,\mathrm{K}\Omega$; $R'_\mathrm{i} = 82\,K\Omega$; $C_\mathrm{f} = 47$ nF, the static gain is 4.75 and the cut-off frequency is 8.67 Hz.

3. Experimental methods

In this section, we present the manufacturing process of the sensor prototype. Then the experimental setup to characterize the effect of the silicone thickness of the sensor is introduced. Also, the experiments that provide different cases of loading for the sensor are described.

3.1. Manufacturing

Layer-by-layer manufacturing methodology [30] described in this section can be extended to any planar arrangement of PZT sensors that can be successively embedded in soft media such as silicone. The following description shows as an example the manufacturing of a sensor which has four PZT (PSI-5H4E) elements arranged in a 2×2 matrix; it is composed of five layers as shown in figure 8. The top (A) and bottom (B) silicone layers are fabricated by spin coating a homogeneous thin layer (0.375 mm) of uncured EcoFlex 50 (Smooth-On, Inc., US). The top (B) and bottom (D) copper-

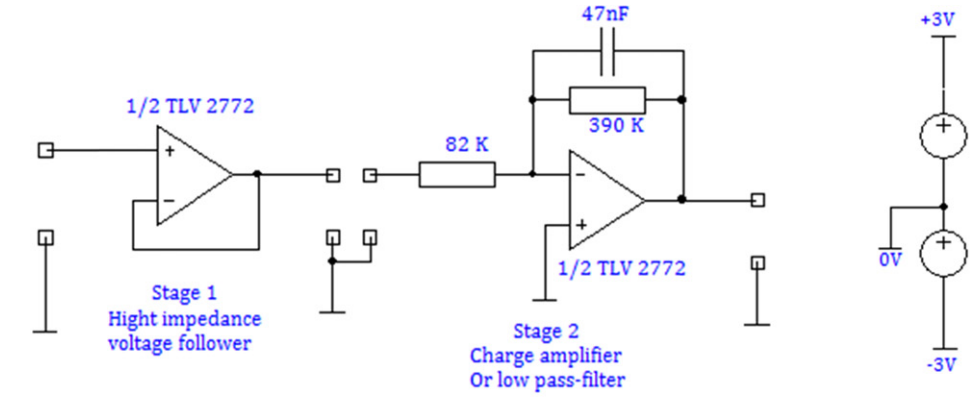

a)

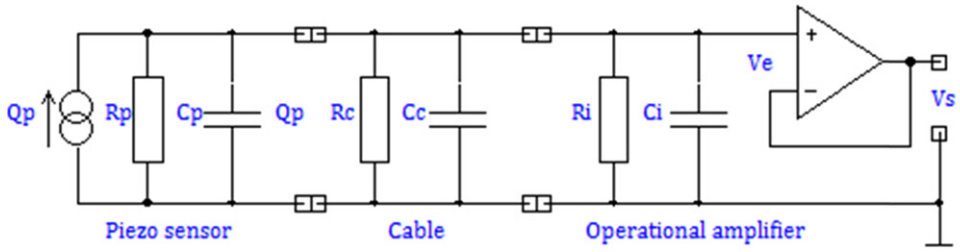

b)

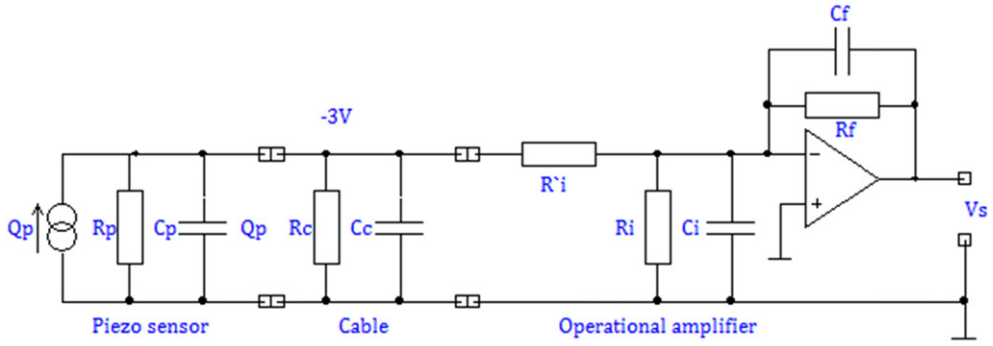

c)

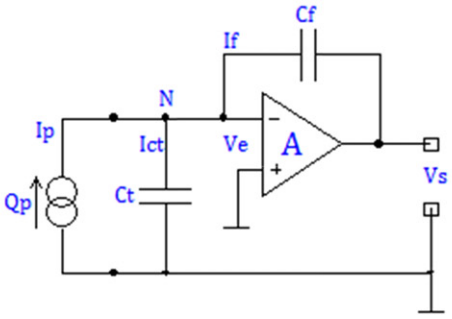

d)

Figure 7. Equivalent signal conditioning circuits to the soft sensors. Piezoelectric sensor signal conditioner schematics (a), stage 1: high impedance follower schematics (b) and stage 2: charge amplifier or low-pass filter schematics (c), the reduction of stage 2 (d).

polyimide layers form a couple of electrodes. They are designed to provide electrical paths for the top and bottom surfaces of each PZT element and insulation. These electrodes are fabricated using laser micromachining (DCH-355-4 UV laser head from Photonics Industries Inc., USA) [31]. Further, the electrode can be designed in order to provide the desired stretchability (i.e. meander paths). The bottom copper-polyimide layer is shared by all PZT elements while the top copper polyimide layer is patterned to provide separate insulated paths for each PZT element. The bottom electrode

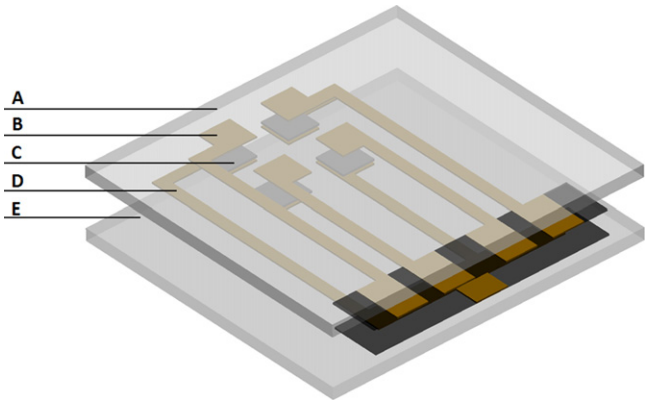

Figure 8. Layers of fabricated 2 × 2 PZT sensor: top silicone layer (A), top copper-polyimide layer (B), 2 × 2 piezoelectric ceramics (C), bottom copper-polyimide layer (D), bottom silicone layer (E).

will provide a common electrical ground while the top electrode will deliver individual signals from each sensing element.

The manufacturing steps for producing the electrodes include the following steps:

- the copper-polyimide sheet is coated with cellulose acetate solution as etching protector;
- the sections of the copper-polyamide sheet where the copper needs to be removed are engraved through laser cut machining and the outline of the electrode is obtained;
- the sheet is then etched with 60% solution of iron III chloride to remove the copper, thus generating a polyimide insulating layer surrounding the other components;
- the sheet is then etched with acetone to remove the etching protector, exposing the copper paths for interfacing the PZT elements and the connector wires;
- the conductive paths are glued to the top and bottom surfaces of the PZT elements using silver conductive epoxy glue (CW2460 Chemtronics US) and electrical connections are made by soldering thin wires to the copper paths;
- finally, the PZT elements with the electrodes and conductive paths are sandwiched between top and bottom silicone layers using uncured EcoFlex 50. The fabricated sensor with 2 × 2 PZT elements is shown in figure 9.

3.2. Experimental setup

The experimental setup to evaluate the performance of the sensor elements (figure 10) is designed to provide normal forces on the sensor. It is composed of a spindle drive with a 270:1 gear ratio with a Maxon dc motor to actuate the sensor holder, which is assembled on a rail cart system providing linear motion. The dc motor is interfaced to an encoder; it is connected to an EPOS 2 controller used to apply specific position profiles to the spindle. The system reaches an accuracy of 3.7 nm. The developed sensor is moving linearly and touching the fixed screw which is assembled to an S-type force transducer (HBM S2M/10 N) with a force measurement range of 0–10 N with the sensitivity of 2 mV V^{-1}. A signal conditioning circuit is specifically developed for PZT sensors. The output signals from the circuit are read and recorded through the analogue inputs of a National Instruments (NI USB-6009) DAQ and LabVIEW (National Instruments, US) software was coded.

3.3. Description of experiments

Loading of a single PZT sensor embedded in the silicone has been conducted in order to verify the concepts introduced in section 2.1.2, the possibility of changing the transfer function of the sensor by changing the material thickness, and to evaluate a possible transfer function for different input conditions. Step, impact and cyclic loads have been applied in sequence to PZT sensors without any material embedment and also embedded in silicone layers of different thicknesses (1.5 mm and 2.3 mm); further, loading parameters such as amplitude, impact time range, and frequency have been changed to investigate their influence.

The sensors have been preloaded before the experiments to guarantee the mechanical contact for the whole test duration. In figures 11–13 the applied position input profiles are reported highlighting the parameters that have been changed, more specifically, a displacement D of 4.63 μm has been considered as the minimum input for each test while a minimum position permanence of 150 ms has been employed.

The profiles have been applied to the Maxon spindle drive through the Maxon EPOS Studio software communicating with the EPOS2 motor driver, thus guaranteeing the execution of the position profiles. The sensors' readings have been collected via an NI acquisition board and the results will be presented in the following sections.

We compared the experimental and theoretical results by overlapping the normalized signal trends. We also investigated the signal trends in a function of silicone thickness.

To get optimal readings from the sensor for all the position profiles, a preload has been applied verifying that the contact was kept even for the largest tested displacement. Since the application of the preload results in a deformation of the silicone embedding the sensor, the thickness of the silicon after preloading has been taken into account.

In the experimental tests, two thickness samples (thicknesses 1.5 mm and 2.3 mm) have been preloaded with 2.68 N and 4.2 N, respectively. Considering the elastic module of the silicone as 0.08 N mm^{-2} and the force contact area on the sensor of 100 mm^2 (see figure 9), resulting silicone thicknesses of 1 mm and 1.11 mm have been used for the theoretical values calculation.

4. Results and discussion

In this section we report on the results of the experimental tests of the sensor prototypes. The results have been grouped in: single sensor readings relative to applied position profiles, distributed sensor sequential and multiple readings in

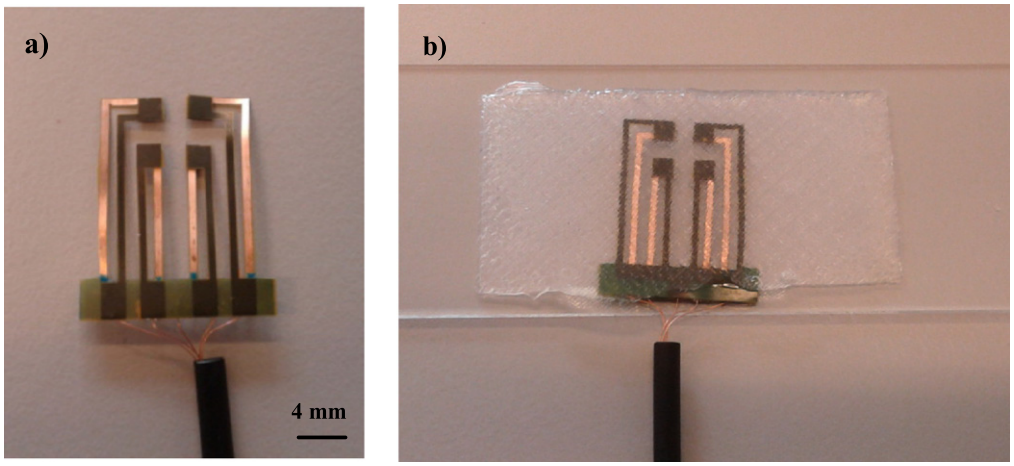

Figure 9. Photograph of fabricated 2 × 2 PZT sensor with copper-polyimide sheets at the top and bottom surfaces of PZT elements (a) and the photo of a 2 × 2 PZT sensor embedded in thin silicone layers (b).

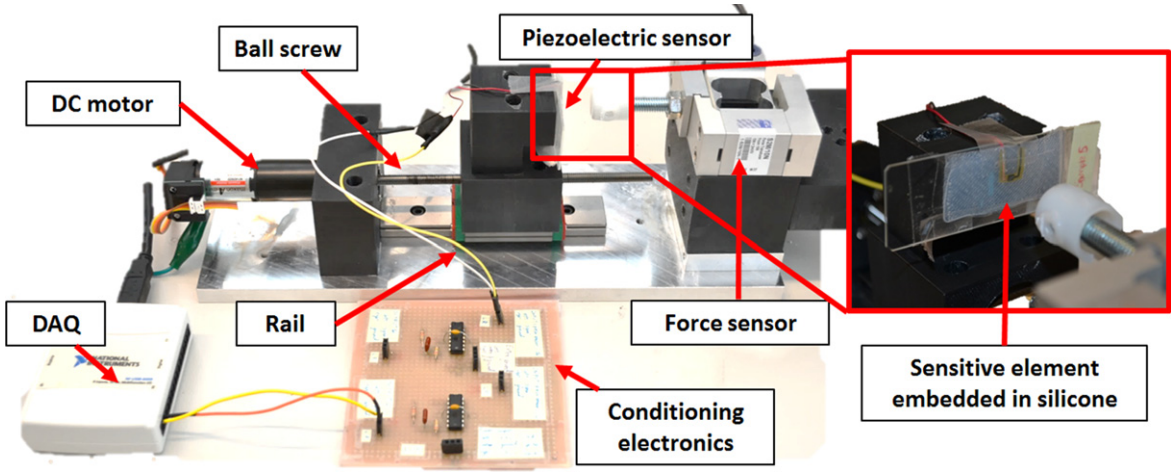

Figure 10. Experimental setup for characterizing the PZT sensors embedded in silicone.

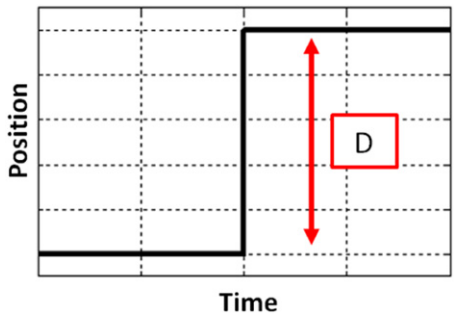

Figure 11. Position profile of the step input, the amplitude has been varied from *D* to 10 times *D* in ten equally spaced values.

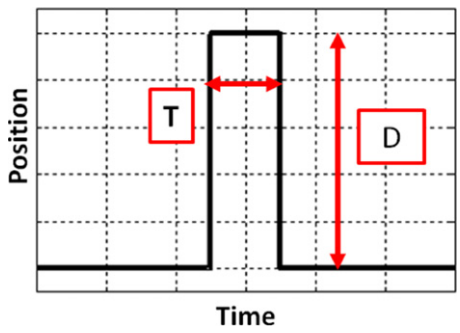

Figure 12. Position profile of the impact input, amplitude has been varied from *D* to 10 times *D* and time *T* has been varied from 150 ms to 250 ms.

different loading conditions, reading of the distributed sensor due to sliding of a load on its surface.

4.1. Characterization of the sensor

The sensor embedment into silicone is supposed to produce two main effects: the compensation for the defects due to the manufacturing process (i.e. since the silver glue is applied manually on the piezoelectric material surface, nonuniform distribution generates stress concentration resulting in a very noisy output) and the modification of the sensor transfer function (thicker silicone, lower signal/force slope).

From the tests, the first feature that is immediately clear is that with the applied position profiles, ranging from 4.6–46 μm, the repeatability of the sensor embedded in silicone is much better than the one not embedded (the coefficient of

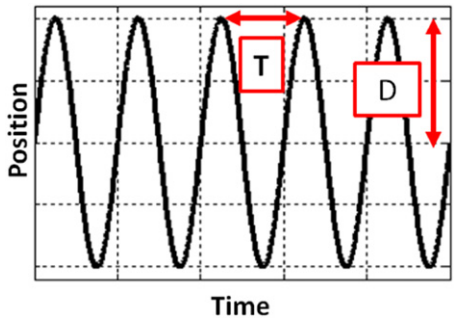

Figure 13. Position profile of the cyclic input, amplitude has been varied from *D* to 6 times *D*, period *T* has been varied from 200 to 500 ms.

determination, R^2, is higher than 0.99; see table 2) the one of the sample embedded. This result is in agreement with the expected behavior, since the silicone compensates for small fabrication defects, distributing the load uniformly on the sensor surface.

Figure 14 reports the sensor response to step input for different loads with different thicknesses of silicone for covering the sensing element. The amplitude A1 is normalized with respect to the maximum input of the DAQ (3 V) is reported. The tests have been repeated five times for each load. The result from the sensor without silicone embedment is reported only for the step response due to its high variability and values that make the comparison with the other cases difficult. The lower slope of the thick silicone case confirms the expected trend discussed in section 2.2 and figure 5.

Another important consideration is to distinguish different loading conditions. The sensor response to step input is characterized by a single amplitude (A1) which, in the case of an impact sensor response, is asymmetric with two characteristic values (A1 and A2), while in case of a cyclic load the response is symmetric. In each case, the response rate for the thinner silicone layer is always higher than the response for the thicker one, as depicted in figures 14–16.

Finally, figure 17 illustrates the interpolation for the different loading conditions and input type grouped according to silicone layer thickness. From figure 17, it is evident that the 10% change in curve steepness is due to the different silicone layer thickness, thus demonstrating the capability of the material in influencing the sensor transfer function (See appendix for the coefficients of the transfer functions).

From the models discussed in section 2.2 (equations (12)–(17)), it is found that the material and geometric properties of the host material influence the transfer function of the sensor. These results on the single PZT embedded in silicone show the feasibility of tuning these transfer functions of the sensor by regulating the thickness of the silicone.

In addition to the robust and repeatable behavior of the sensor, the silicone substrate further enables decoupling and deciphering of the three main contact events (step, impact, and cyclic) by analyzing sensors response symmetry. The results show that the transfer function (force-voltage) is dependent on the loading category (step, input, cyclic) and it is observed that a small range of the cyclic frequency (2–5 Hz) caused no changes in the signal amplitude.

4.2. Distributed PZT sensor results

The proposed design and manufacturing methodology make possible the realization of distributed miniaturized tactile sensors allowing customization, tunable sensitivity and, more importantly, softness and flexibility. The developed sensor which is composed of a 4×2 array of PZT elements embedded in silicone is tested for the localization of contact forces. The forces applied on the sensor manually and the localization of the applied forces is achieved by the measurement of the voltage outputs from each PZT sensitive element (sensel). Figures 18–20 present different types of manual touch on the sensor and the visualization window to distinguish the voltage outputs of each PZT element. The visualization codes the sensor's output in grayscale, where black corresponds to no signal, and white to the maximum signal. The normalized voltage result for each PZT element is presented and the expected stress distributions on the surface where PZT elements are bonded have been simulated in COMSOL.

Single PZT loads have been performed by touching on sensel 1 (one PZT element of the array, numbered 1–8 in figure 18(a)) as in figure 18. It is observed that only the first PZT element is activated at the time of applying force. The sensel 2 is activated after two seconds; the events are very easy to distinguish from the graph showing the good specificity of the sensor.

Figure 19 presents the results for the applied force on the gap between two PZT elements. It is expected that sensel 2 and sensel 6 will be active, which is also observed in the normalized voltage output results.

Another experiment regarding the contact force localization has been implemented by applying force on silicon between four PZT elements as shown in figure 20. According to the location of the contact force, sensels 3, 4, 7 and 8 are expected to be active, which is observed in the experiments. The voltage outputs of sensels 3 and 4 are higher than those of sensels 7 and 8 because the force has been applied closer to sensels 3 and 4, which shows the good localization capabilities of the sensor. The sensor provides continuous spatial information even if composed of discrete elements since, even when the precise location of the sensel is not under loading, the silicone substrate can transfer the load to give significant information on force distribution.

In addition to testing the contact force localization, another experiment has been performed by sliding a part with a wavy surface on the sensor with the dc motor. Figure 21 shows the experiment with the corresponding visualization of the PZT voltage outputs at that instant of time. The part that simulates moving contact is sliding from left (sensel 1 and sensel 5) to right (sensel 4 and sensel 8). If we examine the normalized voltage output plots in figure 21(b) it is observed that the activation of the PZT elements is in the right order as the part is sliding on the sensor. This demonstrates the

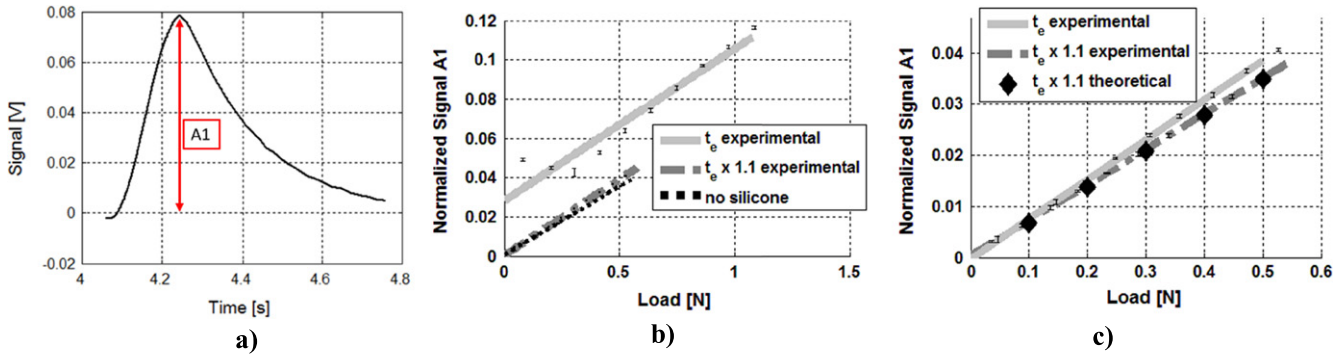

Figure 14. Typical sensor response to the **step input** (a), comparison of the amplitude A1 between different silicone thicknesses, including the case of no-silicone layer (b), evidence of the different transfer function consequent to the different silicone thickness (c). In all the figures, we report the trend expected for the 2.3 mm thickness ($t_e \times 1.1$).

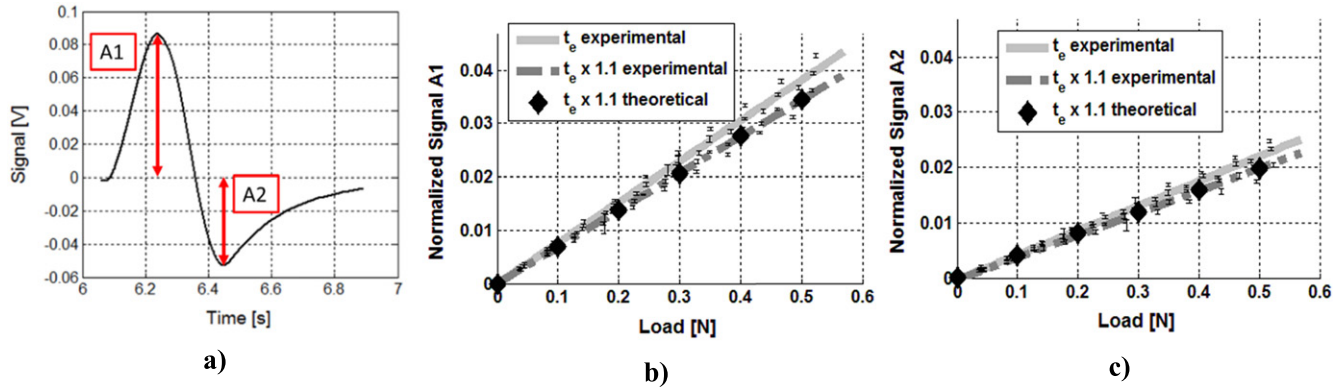

Figure 15. Typical sensor response to the **impact input** (a), comparison of the amplitude A1 between two different silicone thicknesses (b), comparison of the amplitude A2 between two different silicone thicknesses (c). The impact response is characterized by the asymmetry in amplitudes A1 and A2 and all the figures report on the trend expected for the 2.3 mm thickness ($t_e \times 1.1$).

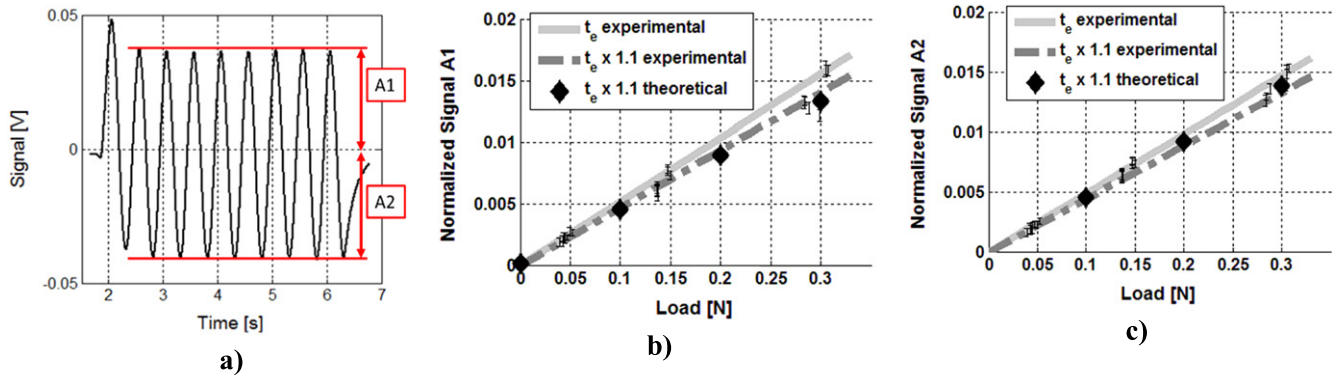

Figure 16. Typical sensor response to the **cyclic input** (a), comparison of the amplitude A1 between two different silicone thicknesses (b), comparison of the amplitude A2 between two different silicone thicknesses (c). The cyclic response is characterized, excluding the first cycle that can be assimilated to an impact, by the symmetry in amplitude A1 and A2, and all the figures report the trend expected for the 2.3 mm thickness ($t_e \times 1.1$).

possibility of evaluating shear forces on the sensitive surface. The activation sequence of the sensels for each column of the sensor is not in the same direction due to the irregularities of the surface of the part that was sliding on the sensor. For the first column the activation order is from bottom to top (first sensel to fifth sensel) whereas the activation order is from top to bottom for the second column (sixth sensel to second sensel). The surface of a tool designed for the purpose (the opposite side is seen as a white block) creates various shearing effects on the surface, as seen in figure 21(a). When pulled (or 'dragged') on top of the sensor surface, the tool highlights the small misalignments during the motion and each PZT sensel generates a signal response with high sensitivity.

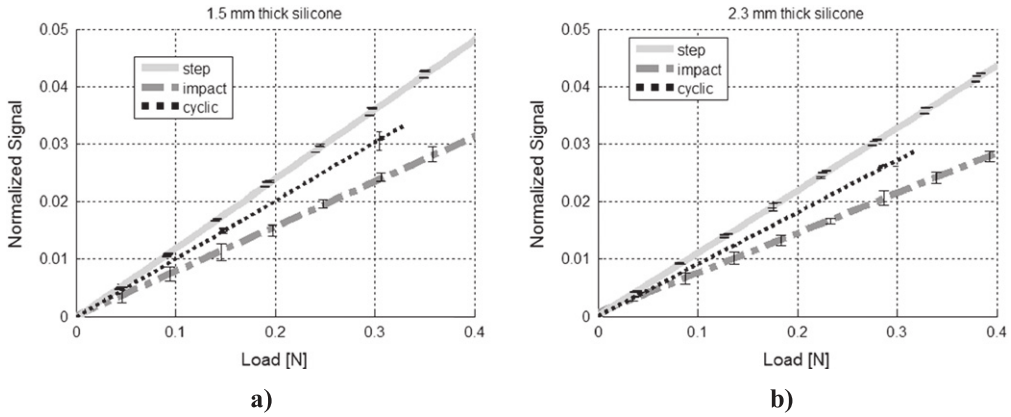

Figure 17. Sensor response A1 + A2 to the step, impact and cyclic inputs for different loads and different silicone thicknesses. Results relative to the 1.5 mm thick silicone are reported in (a), while the results relative to the 2.3 mm thickness are reported in (b). The separation of the characteristic curves and their low standard deviation is evident.

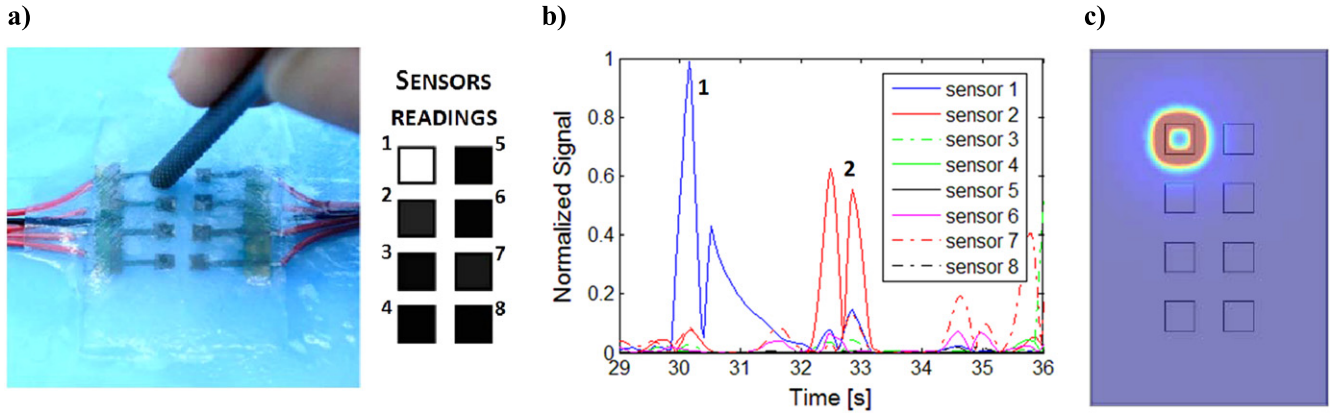

Figure 18. Touching on the first PZT element with the corresponding visualization of each PZT element simultaneously (a): showing expected sensel 1 as the only active sensor at the time of the applied force, normalized PZTs output (b), expected loading position and stress distribution on the surface of the PZTs (c).

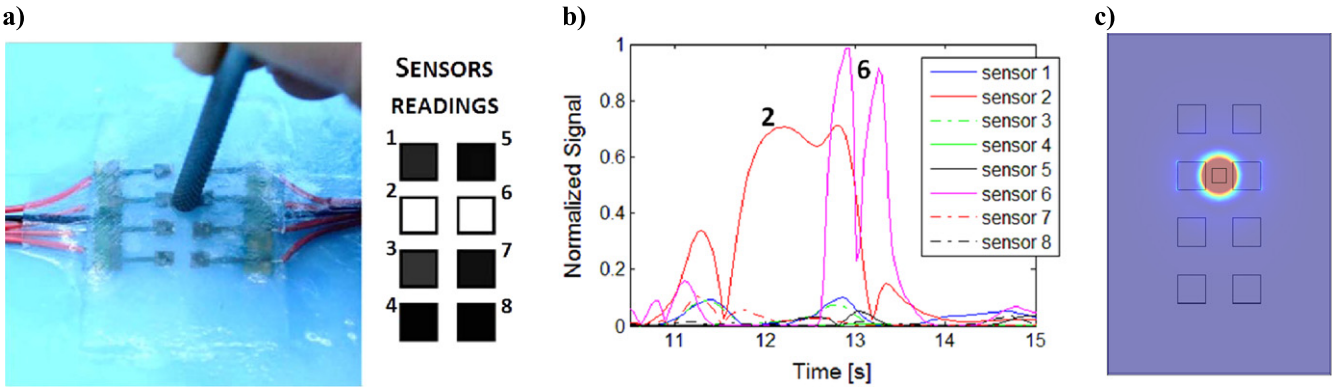

Figure 19. Touching between sensel 2 and sensel 6 with the corresponding visualization of each PZT element simultaneously (a): showing the expected active PZT sensors at the time the force is applied, then normalized PZTs output (b), and loading position and expected stress distribution on the surface of the PZTs (c).

5. Conclusion

This paper presents an innovative design and methodology for the manufacture of robust soft sensors that have a potential for high spatial resolution (with 1.5 mm sensels it can go up to 25 sensels cm^{-2}) and force resolution (up to 50 mN in the tested prototype) thanks to the sensitivity of PZT elements, and stretchability (up to 300% with a proper design) and flexibility thanks to the soft substrate features and to the low profile (under 100 μm) electrode design. The characterization of the sensor and its transfer function is investigated with the application of step, impact and cyclic position profiles and the

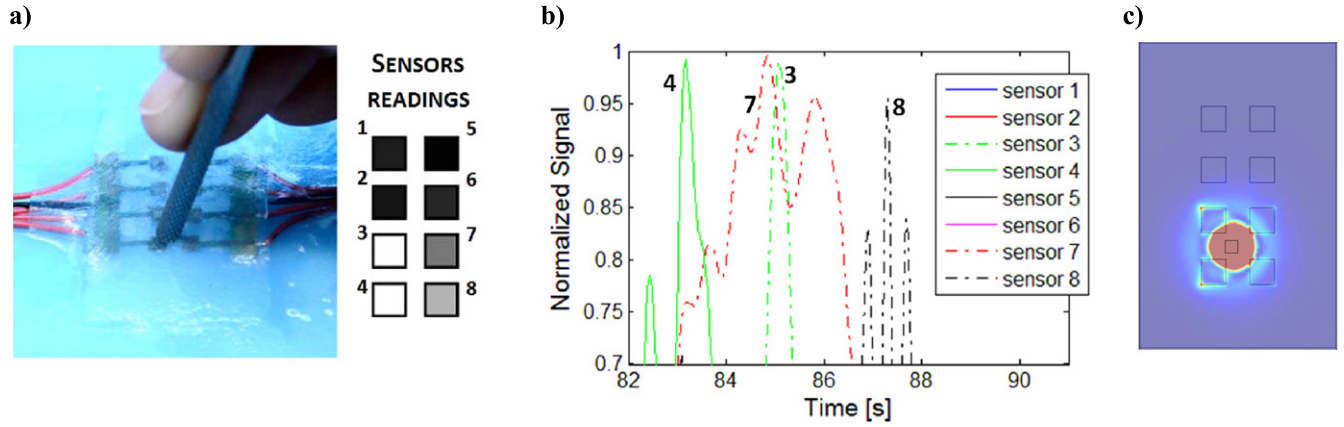

Figure 20. Touching between four PZT elements and close to sensels 3 and 4 with the corresponding visualization simultaneously (a); showing the active PZT elements and that the voltage output of sensels 3 and 4 is higher than that of sensels 7 and 8, the normalized PZTs output (b) and expected stress distribution on the surface of the PZTs (c).

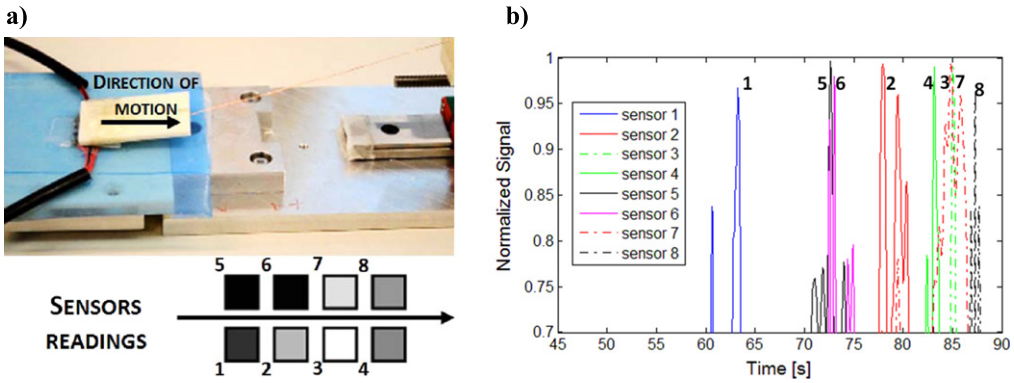

Figure 21. Sliding part on the sensor with the visualization of voltage outputs of each PZT element simultaneously (a) and normalized voltage outputs of each PZT element during the sliding of the part (b).

relative output signal has been collected and analyzed. The changes in the transfer function due to the thickness change in the embedding material are presented.

The developed sensor allows the localization of the contact forces with high reliability thanks to the high sensitivity of the piezoelectric element. Although the sensor is composed of discrete sensitive elements it can sense forces along the distributed surface continuously since the silicone transmits the stress to surrounding elements. Qualitative tests on the sliding force on the distributed sensing surface show promising results since shearing forces are generated on the surface of the PZTs that are bonded inside the elastic material. Due to this, we are able to not only measure 'regular' normal forces on each sensels but also shear forces on them. Consequently, the sensitivity of the surface is much higher for each PZT element. Therefore, the developed sensors show a very promising applicability in a soft, flexible, even stretchable, working environment. The proposed methodology for the soft sensor can be used for developing highly sensitive soft skins for robots, instruments, and even for humans, in order to provide environmental interaction information and integration.

In future work, we plan to consider the system preloading in the modelling of the sensor and to evaluate the time delay induced by the damping of the material in the sensors readings. Eventually, a low dynamic sensing element could be included in the system in order to measure sensor preloads, thus including its contribution in the transfer function. Once the modelling part is more robust, we propose to utilize the force outputs from the PZT elements in the distributed sensor with the final goal being to detect the stiffness of objects.

Acknowledgments

This research is supported by Swiss National Centers for Competence in Research (NCCR) in Robotics and Higher Education Council of Turkey. The authors would also like to thank Amir Firouzeh for his help with the laser manufacturing.

Appendix

The signal and load transfer functions for these sensors can be based on the sum of the amplitudes A1 and A2. The following table lists the coefficients 'a' of the linear interpolation 'normalized signal = a x load' and the relative coefficient of determination R^2.

Table 2. Coefficients of the transfer function describing amplitude change due to different inputs and the silicone substrate thickness.

	Position profile applied					
	Step		Impact		Cyclic	
Silicone thickness (mm)	1.5	2.3	1.5	2.3	1.5	2.3
a	0.0778	0.0695	0.1208	0.1086	0.1014	0.0902
R^2	0.9996	0.9996	0.9994	0.9996	0.9993	0.9984

References

[1] Girão P S, Ramos P M P, Postolache O and Pereira J M D 2013 Tactile sensors for robotic applications *Measurement* **46** 1257–71

[2] Yousef H, Boukallel M and Althoefer K 2011 Tactile sensing for dexterous in-hand manipulation in robotics—a review *Sensors Actuators* A **167** 171–87

[3] Silvera-Tawil D, Rye D and Velonaki M 2014 Artificial skin and tactile sensing for socially interactive robots: a review *Robot. Auton. Syst.* **63** 230–43

[4] Tiwana M I, Redmond S J and Lovell N H 2012 A review of tactile sensing technologies with applications in biomedical engineering *Sensors Actuators* A **179** 17–31

[5] Konstantinova J, Jiang A, Althoefer K, Dasgupta P and Nanayakkara T 2014 Implementation of tactile sensing for palpation in robot-assisted minimally invasive surgery: a review *IEEE Sensors J.* **14** 2490–501

[6] Staudacher E M, Gebhardt M and Dürr V 2005 Antennal movements and mechanoreception: neurobiology of active tactile sensors *Adv. Insect Physiol.* **32** 49–205

[7] Lu N and Kim D 2014 Flexible and stretchable electronics paving the way for soft robotics *Soft Robotics* **1** 53–62

[8] Heo J-S, Kim J-Y and Lee J-J 2008 Tactile sensors using the distributed optical fiber sensors *ICST: Proc. of the 3rd Int. Conf. on Sensing Technology* pp 486–90

[9] Yamada Y, Morizono M, Umetani U and Takahashi T 2005 Highly soft viscoelastic robot skin with a contact object-location-sensing capability *IEEE Trans. Ind. Electron.* **52** 960–8

[10] Kim K, Lee K R, Kim W H, Park K-B, Kim T-H, Kim J-S and Pak J J 2009 Polymer-based flexible tactile sensor up to 32 × 32 arrays integrated with interconnection terminals *Sensors Actuators* A **156** 284–91

[11] Missinne J, Bosman E, Van Hoe B, Van Steenberge G, Kalathimekkad S, Van Daele P and Vanfleteren J 2011 Flexible shear sensor based on embedded optoelectronic components *IEEE Photon. Technol. Lett.* **23** 771–3

[12] Ma C-W, Hsu L-S, Kuo J-C and Yang Y-J 2014 A flexible tactile and shear sensing array fabricated by novel buckypaper patterning technique *2014 IEEE 27th Int. Conf. on Micro Electro Mechanical Systems (MEMS)* pp 441–26

[13] Canavese G, Stassi S, Fallauto C, Corbellini S, Cauda V, Camarchia V, Pirola M and Pirri C F 2014 Piezoresistive flexible composite for robotic tactile applications *Sensors Actuators* A **208** 1–9

[14] Wang H, Zhou D and Cao J 2014 Development of a skin-like tactile sensor array for curved surface *IEEE Sensors J.* **14** 55–61

[15] Hammond F L, Kramer R K, Wan Q, Howe R D and Wood R J 2014 Soft tactile sensor arrays for force feedback in micromanipulation *IEEE Sensors J.* **14** 1443–52

[16] Vogt D M, Park Y-L and Wood R J 2013 Design and characterization of a soft multi-axis force sensor using embedded microfluidic channels *IEEE Sensors J.* **13** 4056–64

[17] Noda K, Matsumoto K and Shimoyama I 2014 Stretchable tri-axis force sensor using conductive liquid *Sensors Actuators* A **215** 123–9

[18] Ponce Wong R D, Posner J D and Santos V J 2012 Flexible microfluidic normal force sensor skin for tactile feedback *Sensors Actuators* A **179** 62–9

[19] Sirohi J and Chopra I 2000 Fundamental understanding of piezoelectric strain sensors *J. Intell. Mater. Syst. Struct.* **11** 246–57

[20] Qasaimeh M A, Sokhanvar S, Dargahi J and Kahrizi M 2009 PVDF-based microfabricated tactile sensor for minimally invasive surgery *J. Microelectromechan. Syst.* **18** 195–207

[21] Seminara L *et al* 2013 Piezoelectric polymer transducer arrays for flexible tactile sensors *IEEE Sensors J.* **13** 4022–9

[22] Kim M-S, Ahn H-R, Lee S, Kim C and Kim Y-J 2014 A dome-shaped piezoelectric tactile sensor arrays fabricated by an air inflation technique *Sensors Actuators* A **212** 151–8

[23] Bentley J 2004 *Principles of Measurement Systems* (Harlow: Pearson Prentice Hall)

[24] Webster J G 2009 *Medical Instrumentation Application and Design* (Hoboken, NJ: Wiley)

[25] Wang X D and Huang G L 2008 On the dynamic behavior of piezoelectric sensors and actuators embedded in elastic media *Acta Mech.* **197** 1–17

[26] Jin C, Han L, Huang G and Wang X 2013 On the dynamic behaviour of surface-bonded piezoelectric sensors/actuators with partially debonded adhesive layers *13th Int. Conf. on Fracture (Beijing, China)*

[27] Huang G L and Sun C T 2006 The dynamic behaviour of a piezoelectric actuator bonded to an anisotropic elastic medium *Int. J. Solids Struct.* **43** 1291–307

[28] Huang G, Song F and Wang X 2010 Quantitative modeling of coupled piezo-elastodynamic behavior of piezoelectric actuators bonded to an elastic medium for structural health monitoring: a review *Sensors* **10** 3681–702

[29] Guyomar D, Wanga X J, Petit L, Lallart M, Monnier T, Yuse K and Audigier D 2011 Modeling of transient bending wave in an infinite plate and its coupling to arbitrary shaped piezo elements *Sensors Actuators* A **171** 93–101

[30] Firouzeh A and Paik J 2015 Robogami: a fully integrated low-profile robotic origami *J. Mechanisms Robotics* **7** 021009

[31] Firouzeh A, Sun Y, Lee H and Paik J 2013 Sensor and actuator integrated low-profile robotic origami *IEEE/RSJ Int. Conf. on Intelligent Robots and Systems (IROS)* pp 4937–44